RAL Report
RAL-94-101

radi
spec
ap

Radio-Frequency Techniques at the ISIS Pulsed Muon Source

S P Cottrell B Hitti and C A Scott

September 1994

Rutherford Appleton Laboratory Chilton DIDCOT Oxfordshire OX11 0QX

Radio-Frequency Techniques at the ISIS Pulsed Muon Source

S.P. Cottrell, B. Hitti, C.A. Scott - September 6, 1994

ISIS Facility, Rutherford Appleton Laboratory,

Engineering and Physical Sciences Research Council.

muon pulses, data can be measured to long times. These advantages have been exploited by Kitaoka *et al* (1982) to directly observe the time evolution of the muon polarisation in the rotating frame.

This report describes experiments performed at the ISIS pulsed muon facility with a view to the future development of an RF μSR facility. After a brief introduction to the principles of the magnetic resonance experiment, the design of the high-power pulsed RF equipment is discussed. Because the longitudinal field strength was limited to approximately 140G, with the corresponding resonance frequency for μ^+ below the base frequency of our power amplifier, studies were restricted to muonium systems with results being presented both for quartz and boron nitride. Finally, both the RF field strength and homogeneity are evaluated using time differential data taken at resonance in the rotating frame.

2. Resonance Concepts

The principles underlying the muon resonance experiments described in this report are closely related to those of continuous wave magnetic resonance, the theory of which has been extensively reviewed by Abragam (1961).

If a static magnetic field, $\mathbf{B_0}$, is applied along the z-axis, collinear with the muon beam and spin polarisation, the muon, having a magnetic moment **M**, will experience a torque and undergo motion described by the equation

$$\frac{d\mathbf{M}}{dt} = \gamma \mathbf{M} \times \mathbf{B}_0 \tag{1}$$

resulting in the spin precessing about the main field at the Larmor frequency $\omega_0 = -\gamma B_0$, where γ is the appropriate magnetogyric ratio.

If an RF field, $\mathbf{B_1}$, is now applied perpendicular to the main field and rotating about it with an angular frequency ω, equation (1) becomes

$$\frac{d\mathbf{M}}{dt} = \gamma \mathbf{M} \times (\mathbf{B}_0 + \mathbf{B}_1(t)) \tag{2}$$

The motion is now considerably more complex and, in practice, easiest to describe by making a transformation to a rotating reference frame (RRF) locked to the frequency of the RF field and having its z-axis collinear with $\mathbf{B_0}$ (i.e. $B_0\mathbf{k}'$). In this new frame of reference the time dependance on the right side of equation (2) is removed and the muon spin will experience an effective field, $\mathbf{B_{eff}}$, given by the equation

$$\mathbf{B_{eff}} = \left(B_0 - \frac{\omega}{\gamma} \right) \mathbf{k}' + B_1 \mathbf{i}' \tag{3}$$

where ω / γ is a fictitious field introduced by the co-ordinate transformation and **i'** and **k'** are unit vectors in the RRF, the situation is shown in figure 1.

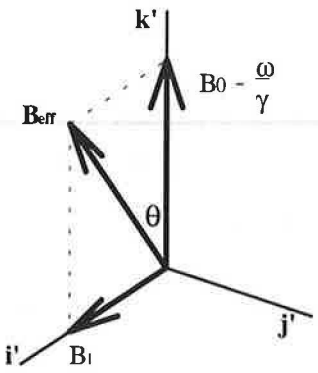

Figure 1 - The rotating frame.

The muon spin will now precess about this effective field with an angular frequency $\omega_{eff} = -\gamma B_{eff}$ which at resonance is equal to $\omega_1 = -\gamma B_1$.

The time evolution of the muon polarisation projected along the z-axis is given by

$$P_z(t) = P_0 \left[\cos^2(\theta) + \sin^2(\theta) \cos(\gamma B_{eff} t) \right] \tag{4}$$

where $\theta = \sin^{-1}\left(\frac{B_1}{B_{eff}} \right)$ and P_0 is the initial polarisation.

The muon experiment is performed in longitudinal geometry, with counters positioned forward (upstream at ISIS) and backward relative to the initial muon polarization. The time dependence of the positron count rate in the detectors is given by the expression

$$N_{F/B}(t) = \frac{N_0}{\tau} e^{-t/\tau}[1 \pm A P_z(t)] \tag{5}$$

where N_F and N_B are the forward and backward count rates respectively, τ is the muon lifetime and A the initial asymmetry. Relaxation effects are assumed to be negligible within the muon lifetime.

The data collected during the experiments can be analysed in two ways, firstly by the time integral method and secondly using a time differential scheme. The former is implemented by defining an RF asymmetry, A_{RF}, in terms of the time integral counts, $\overline{N}$, as follows

$$A_{RF} = \frac{\overline{N}_F^{ON} - \overline{N}_F^{OFF}}{\overline{N}_F^{ON} + \overline{N}_F^{OFF}} - \frac{\overline{N}_B^{ON} - \overline{N}_B^{OFF}}{\overline{N}_B^{ON} + \overline{N}_B^{OFF}} \tag{6}$$

where the superscripts ON and OFF designate whether the RF was on or off during data collection, the experiment alternating between the two states to reduce the effects of equipment instability. By integrating equation (5) over time and substituting into (6) a theoretical form for A_{RF} can be obtained

$$A_{RF} = A \frac{\omega_1^2 \tau^2}{1 + \tau^2[(\omega_0 - \omega)^2 + \omega_1^2]} \tag{7}$$

Thus the usual Lorentzian line shape, with a half width at half maximum of $\sqrt{1/\tau^2 + \omega_1^2}$, is obtained as the static field B_0 is swept through the resonance condition. The amplitude at resonance is equal to $A\omega_1^2\tau^2/(1+\tau^2\omega_1^2)$.

The time differential measurement is made by comparing the ratio of the forward and backward counts. At resonance, equation (5) yields

$$\frac{N_F(t) - N_B(t)}{N_F(t) + N_B(t)} = A\cos(\gamma B_1 t) \tag{8}$$

This type of measurement is of particular importance at resonance as it enables a direct measurement of the RF field, B_1, to be made. The damping of the signal will, in the absence of relaxation effects, provide a measure of the B_1 inhomogeneity.

The system studied in this report is that of muonium, a bound (μ^+e^-) system showing very similar properties to hydrogen. Muonium is often formed when a muon is implanted into a non metallic material. The four possible spin combinations of the electron and muon, $|m_e, m_\mu\rangle$, yield four energy states and four allowed transitions. In low fields both the $|½,½\rangle \rightarrow |½,-½\rangle$ and $|½,-½\rangle \rightarrow |-½,½\rangle$ transitions are of approximately the same energy ($\approx \hbar\gamma_e B/2$) and will therefore both be subject to resonance. The magnetogyric ratio for muonium in this regime is approximately $\gamma_e/2$.

2. Experimental Set-up

A diagram of the apparatus used to generate the high power RF field is shown in figure 2.

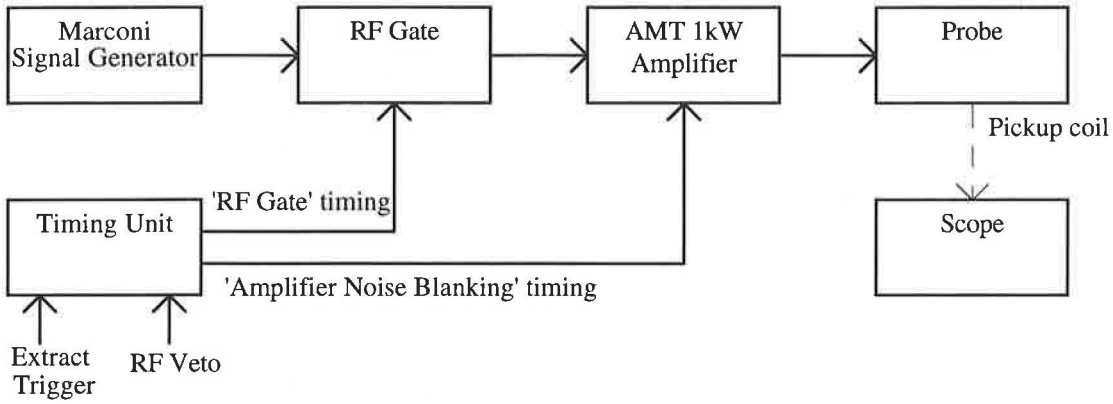

Figure 2 - Block diagram of RF apparatus.

The probe used for the initial experiments consisted of a standard saddle coil wound to provide a cubic access volume of 25mm side and tuned to resonance at 40MHz using a parallel capacitance. A capacitor was placed in series with this tank circuit to act as an impedance transformer and allow the impedance of the complete probe to be matched to 50Ω. To enable the RF field to be monitored during the experiment a 10 turn, 3mm diameter, pickup coil was placed close to the centre of the saddle coil. Since all experiments were conducted at room temperature the probe circuit was simply housed in a aluminium box.

The RF field was produced using a Marconi signal generator, the output of which was gated using a Mini-Circuits RF switch to provide RF pulses of 20μs duration, and an AMT 3200 1kW 6-220MHz power amplifier. To obtain a typical output power of 160W an input level of approximately -15dBm was required.

The sequencing for the experiment was provided by two CAEN NIM timing units synchronised to the 50Hz running of the accelerator by the 'Extract Trigger' signal. An 'RF Veto' input allowed the timing units to be disabled and data to be collected without an RF field. In practice, to reduce problems of equipment instability, data was taken in sets of 500 accelerator pulses alternately with the RF field on and off. Shown in figure 3 is the pulse sequence from the timing units (omitting the 'Amplifier Noise Blanking' timing signal) together with the RF pulse as monitored by the pickup coil and the output of one of the photomultiplier tubes. As shown in the figure, the RF pulse was timed to start after the implantation of the muons in sample. The effect of altering this timing to start the pulse before the arrival of the muons was investigated, with no change in the resonance line being observed.

Longitudinal magnetic fields up to a maximum of 140G were generated using air-cooled Helmholz coils. Four positron detectors with digital counting were used for data collection giving a data rate of approximately 5×10^6 counts/hour.

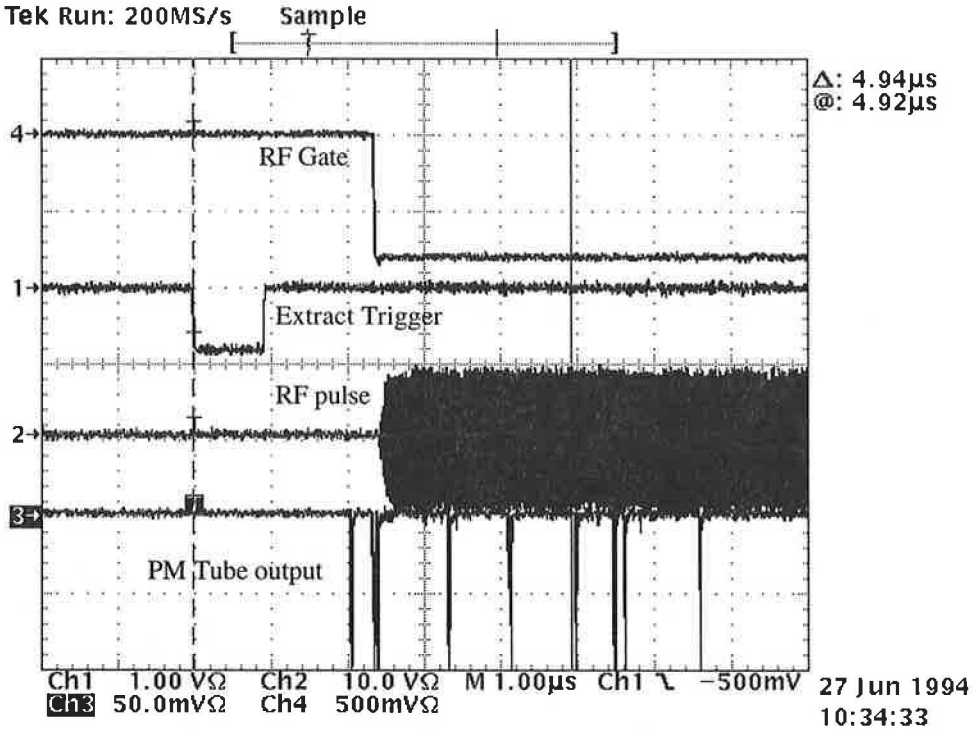

Figure 3 - Timing unit pulse sequence, RF output pulse and photomultipiler tube signal.

3. Results and Discussion

The time integral RF spectra for muonium in quartz taken at 80W and 160W are shown in figures 4(a) and (b) respectively. In each case the longitudinal field scan was started at approximately 19G and incremented in steps of about one third gauss, with 50 data points (each consisting of 0.5×10^6 counts) being taken for the 80W scan. The 160W spectrum is incomplete (only 31 points) because the accelerator failed. For each data point a time integral was performed over the region 0.36μs to 9.32μs as measured from the centre of the muon pulse, and an integral asymmetry obtained using equation (6).

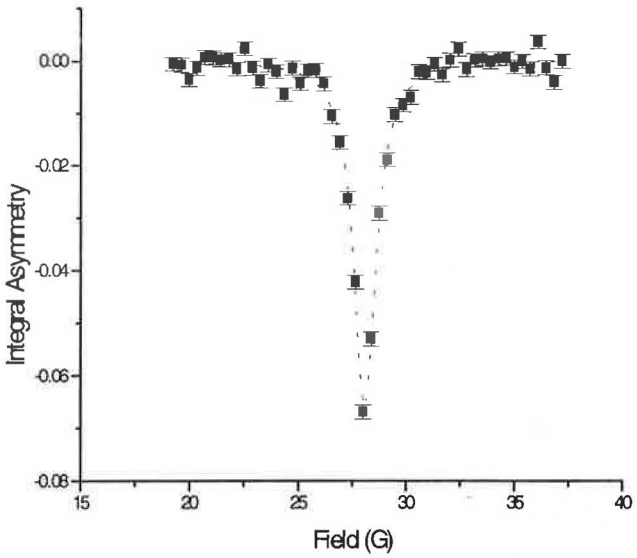

Figure 4(a) - RF μSR of muonium in quartz, 80W.

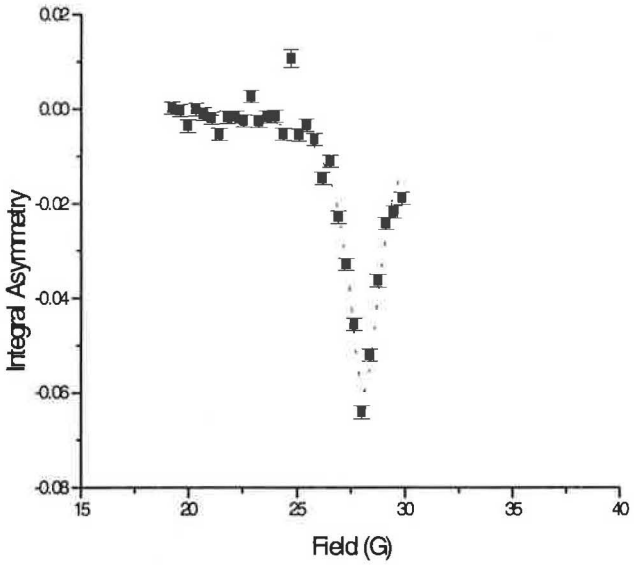

Figure 4(b) - RF μSR of muonium in quartz, 160W.

The field at which resonance occurs, amplitude and half width at half maximum (HWHM) of the spectra have been obtained from a fit to equation (7), these are shown in table 1.

	80W	160W
Resonance Field (G)	28.09 ± 0.01	28.11 ± 0.01
Amplitude	-0.066 ± 0.001	-0.060 ± 0.001
Width (G) (HWHM)	0.61 ± 0.02	0.90 ± 0.03

Table 1 - Resonance parameters for quartz.

At both input powers resonance occurs at a field of 28.1G, in good agreement with the theoretical value of 28.5G. The near constant amplitude of the resonance line at both RF power levels indicates saturation has already occurred at 80W. In this regime $\omega_1 >> \tau^{-1}$ and, from equation (7), the line width will be proportional to ω_1 and consequently the strength of the RF field, B_1. This is confirmed by the data.

Time differential measurements were made at resonance for both the 80W and 160W input power levels, the results are shown in figure 5. A fit to equation (8) gave values for the strength of the RF field, B_1, of 0.63G and 0.82G respectively, in good agreement with the line widths obtained from the time-integral data, but somewhat smaller than the value of 2G obtained using the pickup coil at 160W. The high damping rate observed is indicative of a poor B_1 homogeneity.

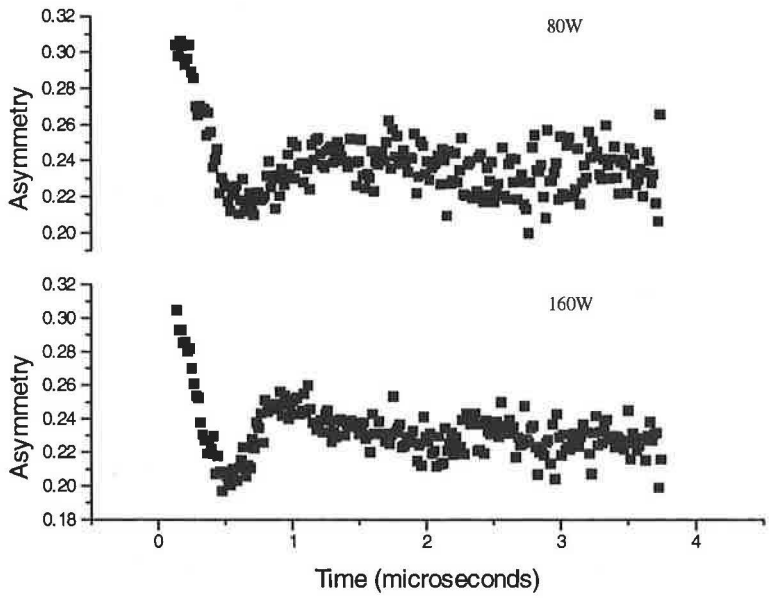

Figure 5 - Time differential measurements of muonium in quartz.
Input power level of 80W (top) and 160W (bottom).

Time integral measurements were also made for muonium in boron nitride, the spectrum is shown in figure 6 with the parameters obtained from a fit to equation (7) shown in table 2. Although resonance occurs at the same field as for the quartz the line is broadened, this is probably because of stronger coupling between the muon and surrounding nuclei.

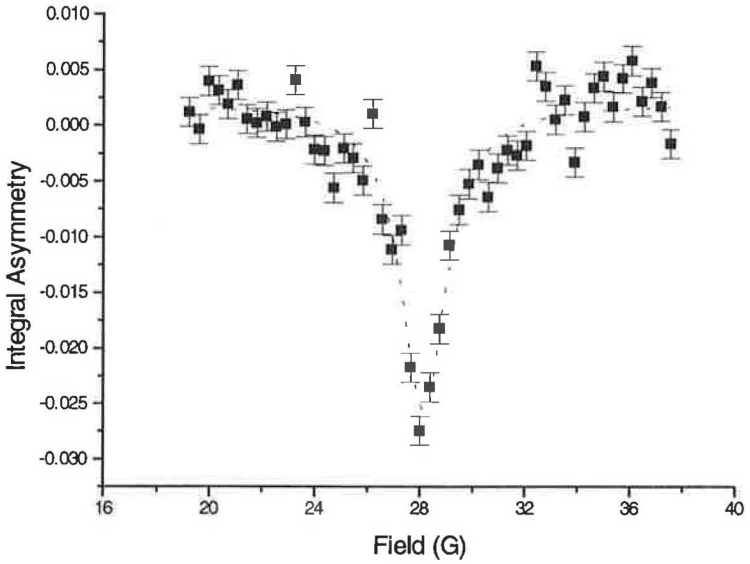

Figure 6 - RF μSR of muonium in boron nitride, 160W

	160W
Resonance Field (G)	28.55 ± 0.03
Amplitude	-0.030 ± 0.001
Width (G) (HWHM)	1.06 ± 0.05

Table 2 - Resonance parameters for boron nitride.

4. Conclusion and Future Work

The objective of the work reported here was to design, construct and prove an RF spectrometer at the ISIS pulsed muon facility. This has been carried out successfully with spectra being obtained for muonium in both quartz and boron nitride, the results are entirely consistent with theoretical predictions. Also demonstrated by the direct observation of B_1 in the rotating frame is the potential for making time differential measurements.

Our goal, however, is the development of an RF facility at ISIS that may be used by external users on a routine basis. Some of the issues that will need addressing if this aim is to be realised are discussed below.

Although adequate for experiments involving muonium, the RF field strength produced by the present probe is rather small and would certainly be insufficient for the study of μ^+, where γ is reduced by a factor of 100. The present RF coil has a large access volume and a correspondingly poor fill factor with our plate-like samples. Consequently, we believe that by optimising the shape of the RF coil to the sample dimensions the situation can be significantly improved. Complementing the effort to increase the RF field strength must be the development of both a high frequency and a broad band probe; each essential for the study of muonium systems in semiconductors (Kreitzmann *et al*). It is intended that the broad band probe will be based upon the delay line design of Lowe and Whitson (1977), and already successfully used for RF μSR by Kreitzmann *et al*. Finally, each probe must be incorporated into a cryostat, ideally providing a temperature range from 4.2K to room temperature.

The spectrometer used to gather the data also requires improvement, principally in the areas of static longitudinal field strength and count rate. The small longitudinal field (less than 140G) produced by the Helmholtz coils restricted investigation to muonium systems; to enable the study of μ^+ a field of at least 1kG should be available . The count rate of 5×10^6counts/hour achieved during the experiments reported here needs be increased, it being only one quarter of the rate used for standard μSR experiments at ISIS. One possible, and expensive, solution would to increase the number of digital detector channels. A cheaper alternative may, however, be to use an analogue detection system similar to that pioneered by Yamazaki *et al* (1982) and already demonstrated at ISIS by teams from Stuttgart and Munich (Hampele *et al* 1994, Münch K-H *et al* 1994).

Acknowledgement

We wish to thank Prof. T L Estle, Dr S F J Cox and Dr W G Williams for their help and support during this project.

5. References

Abragam A 1961 Oxford University Press.

Azuma T, Nishiyama K, Nagamine K, Ito Y, Tabata Y 1986 Hyperfine Interactions **32** 837.

Blazey K W, Estle T L, Rudaz S L, Holzschuh E, Kündig W, Patterson B D 1986 Physical Review B **34**(3) 1422.

Carne A, Cox S F J, Eaton G H, De Renzi R, Scott C A, Stirling G C 1984 Hyperfine Interactions **17-19** 945.

Coffin T, Garwin R L, Penman S, Ledermann L M, Sachs A M 1958 Phys. Rev. **109** 973.

Garwin R L, Lederman L M, Weinrich M 1957 Phys. Rev. **105** 1415.

Hampele M, Herlach D, Kratzer A, Majer G, Major J, Raich H-P, Roth R, Scott C A, Seeger A, Templ W, Blanz M, Cox S F J, Fürderer K 1990 Hyperfine Interactions **65** 1081.

Hampele M, Kratzer A, Maier K, Major J, Münch K-H, Pfiz Th 1994 Proceedings of the 6th Interaction Conference on Muon Spin Rotation/Relaxation/Resonance, Maui.

Kitaoka Y, Takigawa M, Yasuoka H., Itoh M, Takagi S, Kuno Y, Nishiyama K, Hayano R S, Uemura Y J, Imazato J, Nakayama H, Nagamine K, Yamazaki T 1982 Hyperfine Interactions **12** 51.

Kreitzmann S R, Williams D Li, Kaplan N, Kempton J R, Brewer J H 1988 Physical Review Letters **61**(25) 2890

Kreitzmann S R 1990 Hyperfine Interactions **65** 1055.

Kreitzmann S R, Hitti B, Lichti R L, Estle T L, Chow K H To be published.

Lowe I J, Whitson D W 1977 Rev. Sci. Instrum. **48** 268.

Münch K-H, Kratzer A, Kalvius G M, Maier K, Major J, Hampele M, Pfiz Th 1994 Proceedings of the 6th Interaction Conference on Muon Spin Rotation/Relaxation/Resonance, Maui.

Sugai T, Kondow T, Matsushita A, Nishiyama K, Nagamine K 1992 Chemical Physics Letters **188**(1,2) 100

Yamazaki T, Hayano R S, Kuno Y, Ohtake S, Nagae T 1982 Nuclear Instruments and Methods **196** 289.